

EgoForge: Goal-Directed Egocentric World Simulator

Yifan Shen¹, Jiateng Liu¹, Xinzhuo Li¹, Yuanzhe Liu¹, Bingxuan Li¹, Houze Yang¹, Wenqi Jia¹
 Yijiang Li², Tianjiao Yu¹, James Matthew Rehg¹, Xu Cao^{1,†}, Ismini Lourentzou^{1,†}

¹ University of Illinois Urbana-Champaign, ² University of California San Diego

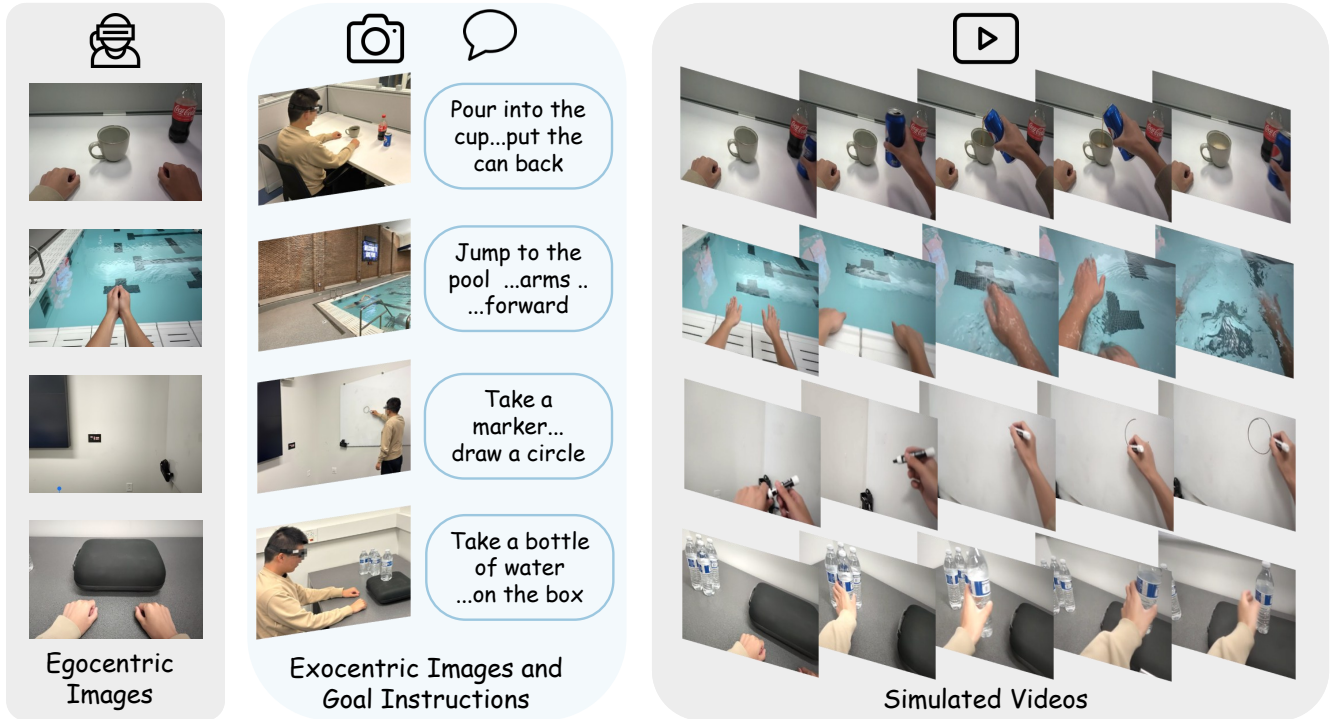


Figure 1: Egocentric video rollouts produced by EgoForge in real-world smart-glasses experiments. Given a single smart-glasses egocentric image, a high-level goal instruction, and an auxiliary exocentric view, EgoForge generates egocentric rollouts that follow user intent and preserve scene structure, without requiring dense supervision, such as camera trajectories, video, or synchronized multi-view capture streams.

Abstract. Generative world models have shown promise for simulating dynamic environments, yet egocentric video remains challenging due to rapid viewpoint changes, frequent hand-object interactions, and goal-directed procedures whose evolution depends on latent human intent. Existing approaches either focus on hand-centric instructional synthesis with limited scene evolution, perform static view translation without modeling action dynamics, or rely on dense supervision, such as camera trajectories, long video prefixes, synchronized multi-camera capture, *etc.* In this work, we introduce **EgoForge**, an egocentric goal-directed world simulator that generates coherent, first-person video rollouts from minimal static inputs: a single egocentric image, a high-level instruction, and an optional auxiliary exocentric view. To improve intent alignment and temporal consistency, we propose VideoDiffusionNFT, a trajectory-level reward-guided refinement that optimizes goal completion, temporal causality, scene consistency, and perceptual fidelity during diffusion sampling. Extensive experiments show EgoForge achieves consistent gains in semantic alignment, geometric stability, and motion fidelity over strong baselines, and robust performance in real-world smart-glasses experiments.

<https://plan-lab.github.io/egoforge>

1. Introduction

Generative world models are redefining how AI systems learn, simulate, and reason about dynamic environments [7, 27, 46]. Recent advances have demonstrated impressive progress in generating realistic natural scenes, such as autonomous driving [57, 88], embodied navigation [5], and virtual worlds [4]. However, despite their visual fidelity and predictive power, these models struggle to model the rich human actions and behaviors found in egocentric vision. This is largely due to the difficulty of modeling first-person streams exhibiting rapid viewpoint changes, frequent hand–object interactions, and complex goal-directed behaviors whose future evolution depends on latent human intent. Beyond visual fidelity, simulating first-person experiences requires understanding physical feasibility, affordances, and procedural dependencies underlying human actions, aspects that traditional frame- or action-conditioned world models overlook.

These limitations have become increasingly important as the demand for immersive and interactive experiences grows across Extended Reality (XR) platforms, including virtual and augmented environments [62, 76, 86]. Such applications require human-centric world models capable of generating predictive, controllable, and physically consistent simulations that support interaction and decision-making. Egocentric world models that are semantically grounded, physically consistent, and dynamically adaptive could enable the next generation of immersive, safe, and responsive digital experiences, improved training environments, and more effective human–AI collaboration.

Existing approaches to egocentric generation [1, 62, 81, 86, 89] face three fundamental limitations: **(1) Dense supervision requirements.** Language or event descriptions are loosely coupled with the visual stream, leading to inconsistencies between described and rendered events. To improve physical consistency, existing methods typically require dense motion annotations, calibrated trajectories, long video prefixes, or synchronized multi-view recordings, which are costly and difficult to obtain at scale, and cannot be assumed reliably at inference time in unconstrained wearable scenarios. **(2) Limited goal-directed control.** Most models condition on short textual prompts or predefined low-level actions (*e.g.*, keyboard or joint controls), producing generic motion patterns and offering limited control over multi-step behaviors. As a result, they struggle to represent semantic human intent such as “open the fridge and pour milk,” or adapt trajectories when higher-level goals change. **(3) Weak physical grounding.** Existing video diffusion models are optimized for visual realism but lack spatial coherence. This lack of 3D awareness prevents consistent reasoning about embodied egocentric motion or object interaction.

To address these challenges, we introduce **EgoForge**, an egocentric world simulator designed for realistic and controllable first-person video generation. Unlike existing approaches that rely on dense motion signals, multi-view capture, or video input, EgoForge generates coherent, goal-directed egocentric rollouts from a single egocentric observation, a high-level instruction, and an optional auxiliary exocentric reference image providing complementary context about scene layout. Built upon a diffusion-transformer backbone, EgoForge incorporates geometry-level grounding to ensure spatial and physical coherence by enforcing representational alignment [71, 79] between the implicitly modeled 3D geometric structure and diffusion latents, thereby encouraging geometry-aware video synthesis. To improve long-horizon rollout behavior and better align generation with task intent, we further propose VideoDiffusionNFT, a trajectory-level reward-guided refinement stage that optimizes goal completion, temporal causality, scene stability, and perceptual fidelity, ultimately enhancing the overall realism and consistency of world simulation.

To evaluate goal-directed world simulation, we curate **X-Ego**, a new benchmark providing egocentric observations paired with rich semantic annotations for grounded, real-world–aligned video generation. Comprehensive experiments demonstrate that **EgoForge** achieves large gains in semantic alignment (+13.5% DINO-Score, +10.1% CLIP-Score ↑) while substantially improving video realism and temporal coherence,

with 43% lower FVD and 51% lower Flow MSE, indicating more realistic and temporally coherent videos compared to strong baselines. EgoForge also yields higher structural fidelity (+9.7% SSIM \uparrow), lower perceptual error (-35% LPIPS \downarrow), and improved reconstruction quality (+17.8% PSNR \uparrow), yielding egocentric rollouts that better follow user intent, exhibit smoother motion, and maintain scene structure over time.

Contributions. The contributions of our work are:

- We introduce **EgoForge**, an egocentric world simulator that generates goal-directed first-person video rollouts from minimal inputs, *i.e.*, a single egocentric image, a high-level instruction, and an optional auxiliary exocentric view. To our knowledge, this is the first work to generate goal-directed egocentric rollouts beyond hand-centric instructional motion from minimal static context (ego/exo images and instruction) without pose/trajectory inputs, video prefixes, or synchronized multi-view capture at inference.
- To improve intent alignment and temporal coherence, we propose **VideoDiffusionNFT**, a novel trajectory-level reward-guided refinement mechanism for video diffusion that fuses goal completion, scene stability, temporal causality, and perceptual fidelity into a unified vector-field update that steers sampling toward coherent, goal-consistent rollouts.
- We curate the **X-Ego** benchmark, pairing egocentric observations with detailed event flows, hand-object interactions, object-state changes, and auxiliary visual references, enabling systematic evaluation of goal alignment, temporal coherence, and physical consistency for controllable egocentric rollouts.

2. Related Work

As summarized in Table 1, prior work either (i) requires costly continuous exocentric video streams for synchronized view generation rather than predictive simulation [31, 75, 83], (ii) performs static image-to-image view translation without modeling temporal action evolution [13, 49], or generates image-conditioned instructional video largely in hand-centric settings, where motion is localized to the hands and nearby manipulated objects and the scene context is largely static [36]. In addition, existing methods achieve broader egocentric video generation by conditioning on explicit motion signals (pose/trajectories/camera paths) or synchronized multi-view exocentric video streams [31, 36, 67, 83]. In contrast, EgoForge formulates egocentric video generation from a single first-person image and instruction, enabling controllable, physically consistent prediction without requiring dense motion supervision.

Egocentric Vision. Egocentric vision research has rapidly advanced with improvements in both dataset quality and model scaling. Foundational benchmarks such as EPIC-KITCHENS [15–17], Ego4D [21], and EgoExo4D [22] have enabled large-scale analysis of daily tasks and multi-view human activity. On the modeling side, prior work focuses on recognizing actions, gaze, attention, and human-object interactions from egocentric views [28, 32, 42, 54, 68], or on estimating human body pose [34, 44, 65]. There is also increasing attention to vision-language models for learning multimodal representations from egocentric

Table 1: Representative Related Works. I/O icons represent  Ego-view,  Ego Video,  Exo Image,  Exo Video stream,  Text/Action prompt, and  Camera parameters. Prior work requires (multi-view) video streams or camera trajectories, while EgoForge generates egocentric video from minimal static observations. \ddagger assumes fixed camera poses. \star hand motion synthesis.

Model	Inputs	Output
4Diff [13]	 + 	
EgoWorld [49]		
Exo2Ego-V [83]	 \times 4 sync	
EgoX \ddagger [31]		
Handi \star [36]	 + 	
EgoDreamer [67]	 +  + 	
EgoForge (Ours)	 +  + 	

data [3, 8, 39, 52, 58] and forecasting plausible hand motions [30], hand-object interactions [78], and gaze [84]. Methods for cross-view exocentric-to-egocentric translation and joint egocentric video-motion synthesis depend on explicit motion supervision, typically in the form of camera trajectories or synchronized multi-camera exocentric recordings [13, 41, 49, 74]. However, such data are difficult to acquire and still fail to capture high-level, goal-driven human intent, limiting controllability and semantic diversity in generated egocentric videos. In contrast, EgoForge generates egocentric videos without requiring motion or view supervision.

Video Generation. Advances in latent diffusion [12, 51, 56] and score-based generative modeling [26, 59, 60] established the principles of iterative denoising and latent-space synthesis that now underpin most video generators. Building on these foundations, transformer-based video diffusion architectures enable greater temporal coherence, longer duration, and improved realism [33, 48, 50, 73]. Large-scale frameworks such as Stable Video Diffusion [6], VideoCrafter [10, 11], and Open-Sora [37], demonstrate strong cross-domain synthesis through efficient latent modeling and scaling. While these video generation models excel at text-conditioned general-purpose video, they lack representations of agent intent, viewpoint dynamics, and causal continuity required for egocentric simulation.

World Models. World models are predictive models learned to simulate the environment dynamics, serving either as tools for agent policy optimization [20, 23, 35] or as high-fidelity world simulators and game engines [2, 7, 9, 43, 63, 80]. Early approaches [18, 24, 72], use environment simulation to train agent policies efficiently, taking advantage of latent imagination or tree search for decision-making [14, 61]. TD-MPC2 [25] and PWM [19] improve scalability, sample efficiency, and generalization to diverse robotic tasks using agent-centric training pipelines. For world simulation, recent efforts in video and scene synthesis, such as Matrix [?], Matrix-Game [86], Cosmos [1], and Aether [89], explore the generation of unlimited and interactive video streams of 3D worlds with fine-grained user control. In parallel, works extend to multi-task settings by utilizing action and task embeddings [25], natural language action descriptions [38, 77], and latent action representations [7]. Recent frameworks improve interaction freedom by decoupling offline world model training from agent policy learning [69], yet offer limited control granularity and lack explicit understanding of user intent and task context. In contrast, EgoForge generates an egocentric video trajectory that fulfills a specified goal, via our proposed VideoDiffusionNFT trajectory-level reward-guided refinement that optimizes goal completion and temporal coherence.

3. Method

EgoForge is an egocentric world simulator designed to generate goal-directed first-person video rollouts that simulate how a scene evolves when a user performs a specified task. Given an initial egocentric frame or short clip $\mathbf{m}x_{1:k}$, the objective is to synthesize a plausible future sequence $\mathbf{m}x_{k+1:T}$. Formally, EgoForge models

$$p_{\theta}(\mathbf{m}x_{k+1:T} \mid \mathbf{m}x_{1:k}) = \prod_{t=k+1}^T p_{\theta}(\mathbf{m}x_t \mid \mathbf{m}x_{<t}, \mathcal{C}), \quad (1)$$

where $\mathcal{C} = \{\mathbf{m}x_{1:k}, y, \mathbf{m}x^{exo}\}$ is the conditioning context, which consists of the embeddings derived from $\mathbf{m}x_{1:k}$, instruction y , and the exocentric reference $\mathbf{m}x^{exo}$. Unlike prior approaches, we do not assume access to camera trajectories, pose signals, or synchronized multi-view streams at inference time. The generated rollout should satisfy three key properties, such as goal alignment (*i.e.*, the sequence reflects the intended instruction), temporal coherence (*i.e.*, motion evolves smoothly across frames), and physical consistency (*i.e.*, scene geometry and interactions remain stable).

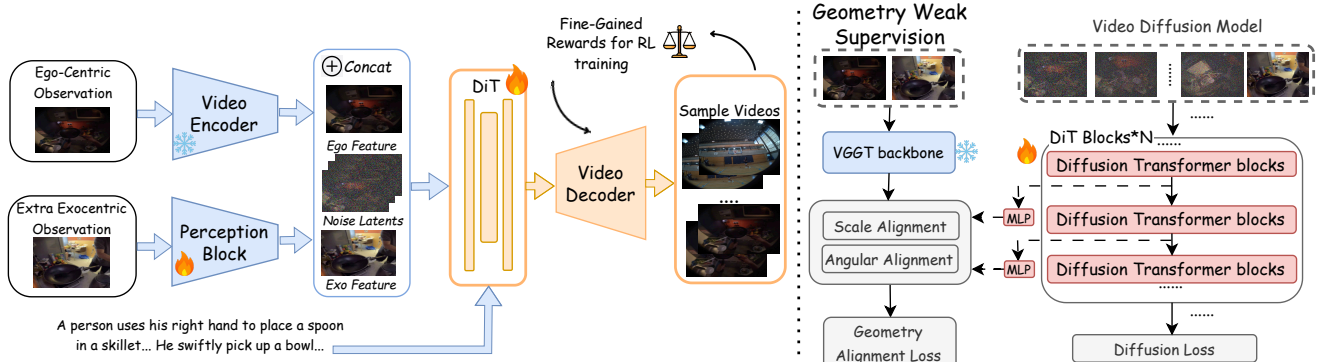


Figure 2: EgoForge Overview: Given a single egocentric observation, a high-level (instruction) intent, and an auxiliary exo-view reference, EgoForge fuses encoded visual features with noisy video latents at each DiT block to guide generation. Geometry alignment weakly supervises intermediate features using angular and scale consistency to encourage spatially stable rollouts. The resulting rollout videos are further refined via a novel VideoDiffusionNFT alignment policy that optimizes goal completion, scene consistency, temporal causality, and perceptual fidelity.

3.1. Diffusion-Based Egocentric Generator

Figure 2 illustrates the overall architecture of EgoForge, where video generation is performed in the latent space of a pretrained video autoencoder. Let $\mathbf{m}z_0 = \text{Enc}(\mathbf{m}x_{k+1:T})$ be the latent trajectory. Following the variance-preserving flow-matching objective [40], we sample a discrete diffusion step $t \sim \mathcal{U}(0, 1)$ and sample noise tensor $\epsilon \sim \mathcal{N}(\mathbf{0}, \mathbf{I})$. The noisy latent is then generated according to the standard diffusion process $\mathbf{m}z_t = \sqrt{\bar{\alpha}_t} \mathbf{m}z_0 + \sqrt{1 - \bar{\alpha}_t} \epsilon$ where $\bar{\alpha}_t = \prod_{s \leq t} \alpha_s$ is the cumulative product of the noise schedule. The reverse process is parameterized by a diffusion transformer:

$$p_\theta(\mathbf{m}z_{t-1} \mid \mathbf{m}z_t, \mathcal{C}) = \mathcal{N}(\mathbf{m}z_{t-1}; \mu_\theta(\mathbf{m}z_t, t, \mathcal{C}), \Sigma_t), \quad (2)$$

where μ_θ is the learned mean of the reverse step and Σ_t is the variance prescribed by the noise schedule. Conditioning on \mathcal{C} is implemented through adaptive normalization and cross-attention layers that incorporate the fused embedding. We concatenate the noisy latent with ego and conditioning context features along the channel dimension $\tilde{\mathbf{m}}z_t = \text{Concat}(\mathbf{m}z_t, \mathbf{f}_{\text{ego}}, \mathbf{f}_{\mathcal{C}})$ and inject the timestep t through a learned time embedding $\gamma(t)$. Following modern diffusion architectures, the denoising objective is a velocity-prediction loss $\mathcal{L}_D = \mathbb{E}_{t, \mathbf{m}z_t, \epsilon} \left[\|\epsilon - v_\theta(\tilde{\mathbf{m}}z_t, t, \mathcal{C})\|_2^2 \right]$, where v_θ is the conditional velocity field.

Geometry Weak Supervision. To inject 3D reasoning into the diffusion backbone, we align its intermediate representations with geometry features extracted from a pretrained VGGT [66], following REPA [79] and Geometry Forcing [71]. Let $\mathbf{g}_l \in \mathbb{R}^{N \times Q \times D_g}$ denote the VGGT features at layer l , where L is the number of selected layers, N and Q index temporal and spatial tokens, and D_g denotes the feature dimension. For the diffusion transformer, we extract hidden activations $\mathbf{h}_l \in \mathbb{R}^{N' \times Q' \times D_h}$ from the corresponding layers. Because the two backbones operate at different resolutions, we introduce a learnable projection operator $\Pi_l: \mathbb{R}^{N' \times Q' \times D_h} \rightarrow \mathbb{R}^{N \times Q \times D_g}$, implemented via spatiotemporal resampling and channel projection, and obtain projected diffusion features $\mathbf{p}_l = \Pi_l(\mathbf{h}_l)$. To encourage the diffusion features to match the direction of VGGT geometry features, we employ a cosine alignment loss

$$\mathcal{L}^{\text{ang}} = - \frac{1}{LNQ} \sum_{l,n,q} \cos(\mathbf{g}_{l,n,q}, \mathbf{p}_{l,n,q}). \quad (3)$$

Moreover, to constrain the magnitude of geometric features and avoid scale collapse, we introduce a scale alignment loss. We first normalize the projected features as $\tilde{\mathbf{p}}_l = \mathbf{p}_l / (\|\mathbf{p}_l\|_2 + \varepsilon)$ and obtain geometry predictions $\hat{\mathbf{g}}_l = \rho_l(\tilde{\mathbf{p}}_l)$ via a learned linear head ρ_l . The scale alignment loss is then defined as

$$\mathcal{L}^{\text{sca}} = \frac{1}{LNQ} \sum_{l,n,q} \|\hat{\mathbf{g}}_{l,n,q} - \mathbf{g}_{l,n,q}\|_2^2. \quad (4)$$

The geometry-level coordination objective aggregates both terms across a selected set of layers $\mathcal{L}_G = \zeta_1 \mathcal{L}^{\text{ang}} + \zeta_2 \mathcal{L}^{\text{sca}}$, where ζ_1 and ζ_2 are coefficients balancing the contributions of angular and scale consistency.

3.2. VideoDiffusionNFT Alignment

Although EgoForge conditions generation on multiple signals, *i.e.*, the observed egocentric input, the instruction text, and an optional exocentric reference image, their influence can be imbalanced during diffusion sampling, leading to cue dominance or inconsistent rollouts. To address this, we introduce VideoDiffusionNFT, a trajectory-level reward-guided refinement that transforms a set of scalar rewards into probabilistic optimality signals that guide policy improvement. Specifically, we extend DiffusionNFT [87] to the video domain and perform negative-aware finetuning with our fine-grained reward functions. Given the supervised-finetuned policy π^{old} , for each condition $c \in \mathcal{C}$ we treat the generated samples $\mathcal{X}_c = \{\mathbf{m}x_{1:T}^{(k)}\}_{k=1}^K$ as rollout candidates under condition c , each associated with reward $\mathcal{R}_{\text{total}}^{(k)}(\mathbf{m}x_{1:T}^{(k)}, c)$, and compute the empirical estimate of the per-condition expected reward $\mu_c = \mathbb{E}_{\mathbf{x} \sim \pi^{\text{old}}(\cdot|c)}[\mathcal{R}_{\text{total}}(\mathbf{x}, c)] \approx \frac{1}{K} \sum_{k=1}^K \mathcal{R}_{\text{total}}^{(k)}(\mathbf{m}x_{1:T}^{(k)}, c)$ and normalize each condition’s reward into an optimality probability defined as

$$\tilde{\mathcal{R}}_{\text{total}}^{(k)} = \frac{1}{2} \left[1 + \text{clip} \left(\frac{\mathcal{R}_{\text{total}}^{(k)}(\mathbf{m}x_{1:T}^{(k)}, c) - \mu_c}{Z_c}, -1, 1 \right) \right], \quad (5)$$

where $Z_c > 0$ is a normalized local reward scale that ensures $\tilde{\mathcal{R}}_{\text{total}}^{(k)} \in [0, 1]$. For notational convenience, we denote the normalized optimality as $r(\mathbf{m}x^{(k)}, c) := \tilde{\mathcal{R}}_{\text{total}}^{(k)}$, so that $r(\mathbf{m}x^{(k)}, c) \in [0, 1]$. To measure how well the policy performs on condition c overall, we compute the expected per-condition optimality mass $p_{\pi^{\text{old}}}(o = 1 | c) := \mathbb{E}_{\mathbf{m}x \sim \pi^{\text{old}}(\cdot|c)}[r(\mathbf{m}x, c)]$ inducing reweighted positive and negative posteriors:

$$\begin{aligned} \pi^+(\mathbf{m}x | c) &= \frac{r(\mathbf{m}x, c)}{p_{\pi^{\text{old}}}(o = 1 | c) + \varepsilon} \pi^{\text{old}}(\mathbf{m}x | c), \\ \pi^-(\mathbf{m}x | c) &= \frac{1 - r(\mathbf{m}x, c)}{1 - p_{\pi^{\text{old}}}(o = 1 | c) + \varepsilon} \pi^{\text{old}}(\mathbf{m}x | c), \end{aligned} \quad (6)$$

where $\varepsilon > 0$ is a small constant to avoid division by zero. By construction, these posteriors satisfy $\pi^+ > \pi^{\text{old}} > \pi^-$ in expected reward. We define reinforcement guidance as a vector field acting on the intermediate forward states $\mathbf{m}z_t$, steering the model toward π^+ while repelling it from π^- .

Let $v^+, v^-,$ and v^{old} denote the velocity fields of the respective policies, and let $\alpha(\mathbf{z}_t, c) = \mathbb{E}[r(\mathbf{x}, c) | \mathbf{z}_t, c]$ denote the conditional optimality at the intermediate state $\mathbf{m}z_t$. The improvement direction is $\Delta(\mathbf{m}z_t, c, t) = [1 - \alpha(\mathbf{m}z_t, c)](v^{\text{old}} - v^-) = \alpha(\mathbf{m}z_t, c)(v^+ - v^{\text{old}})$, yielding the guided target field $v^*(\mathbf{m}z_t, c, t) = v^{\text{old}}(\mathbf{m}z_t, c, t) + \frac{1}{\beta} \Delta(\mathbf{m}z_t, c, t)$, where $\beta > 0$ controls the guidance strength. Finally, we optimize the policy via a negative-aware flow-matching loss

$$\mathcal{L}(\theta) = \mathbb{E}_{c, \mathbf{m}z_t} \left[\rho \|v_\theta^+ - v^*\|_2^2 + (1 - \rho) \|v_\theta^- - v^*\|_2^2 \right], \quad (7)$$

Table 2: Quantitative comparisons on the X-Ego benchmark between EgoForge and other finetuned baseline variants. +EV: with exo-view img, +TT: text-only domain adaptation; +CI: our conditioning inputs (exo-view and goal instructions) with our structured injection with Geometry Weak Supervision.

Model	DINO-Score↑	CLIP-Score↑	SSIM ↑	LPIPS ↓	FVD ↓	flow MSE ↓	PSNR ↑
Cosmos+EV	48.60	29.60	0.67	0.28	485.75	6.82	18.30
Cosmos+TT	50.80	30.40	0.71	0.25	433.90	6.31	18.88
HunyuanVideo+EV	52.80	29.20	0.70	0.27	405.87	6.30	18.61
HunyuanVideo+TT	54.10	29.86	0.72	0.24	365.80	5.95	19.10
WAN2.2+EV	52.91	35.11	0.71	0.27	352.41	6.25	20.05
WAN2.2+TT	54.80	36.20	0.73	0.25	310.57	5.60	20.64
WAN2.2+CI	58.92	38.05	0.76	0.18	218.72	3.92	22.87
EgoForge (Ours)	61.25	39.30	0.79	0.15	182.25	2.83	24.08

where $v^* = v^*(\mathbf{m}z_t, c, t)$ is the guided target field defined above, and $\rho \sim \text{Ber}(\alpha(\mathbf{m}z_t, c))$, and $v_\theta^+ = (1 - \beta)v^{\text{old}} + \beta v_\theta$, $v_\theta^- = (1 + \beta)v^{\text{old}} - \beta v_\theta$. Under this objective, the optimal solution satisfies

$$v_{\theta^*} = v^{\text{old}} + \frac{2r(\mathbf{m}x, c) - 1}{\beta}(v^* - v^{\text{old}}), \quad (8)$$

encouraging the model toward sampling higher-reward rollouts. More information about VideoDiffusionNFT can be found in Appendix A.

Rewards. Given a set of rollout candidates $\mathcal{X} = \{\mathbf{m}x_{1:T}^{(k)}\}_{k=1}^K$, we evaluate each generated video trajectory $\mathbf{m}x_{1:T}^{(k)}$ of length T with a set of scalar rewards that measure goal completion, environment preservation, temporal causality, and perceptual fidelity:

- 🪄 **Goal Completion** ($\mathcal{R}_{\text{goal}}$) evaluates task completion, *i.e.*, whether the trajectory successfully achieves the task outcome, measured by the similarity of the final state to the target reference.
- 🪄 **Scene Consistency** (\mathcal{R}_{env}) measures consistency with the initial scene, penalizing drift, misplaced objects, or transitions into unrelated environments.
- 🪄 **Temporal Causality** ($\mathcal{R}_{\text{temp}}$) assesses whether the motion evolves in a physically plausible, coherent, and causal manner without temporal artifacts.
- 🪄 **Perceptual Fidelity** (\mathcal{R}_{per}) captures overall visual clarity, stability, and absence of distortions or artifacts.

Rewards are combined into a single total reward for each rollout $\mathcal{R}_{\text{total}}^k(x_{1:T}^k)$. We leverage strong vision–language models as non-parametric evaluators to score the generated videos. Complete prompts and detailed design can be found in Appendix B.

4. Experiments

4.1. Experimental Setting

X-Ego Benchmark. We introduce X-Ego, the first large-scale benchmark designed to evaluate egocentric world models on their ability to synthesize complex scenes involving multiple, fine-grained conditioning signals. X-Ego is curated from the Nymeria [45] and Ego-Exo4D [22] datasets. To facilitate a deeper understanding of human–environment interaction, we further enrich this benchmark with dense annotations detailing granular hand–object dynamics, object state changes, and step-level action semantics. The full corpus consists of 15,000 training samples, paired with 100 held-out unseen test clips for standardized

Table 3: Quantitative comparisons on the X-Ego benchmark. EgoForge outperforms all baselines across semantic, perceptual, and temporal metrics.

Model	DINO-Score↑	CLIP-Score↑	SSIM ↑	LPIPS ↓	FVD ↓	flow MSE ↓	PSNR ↑
EgoDreamer [67]	42.35	25.40	0.58	0.35	580.45	8.15	15.20
Handi [36]	31.12	18.25	0.42	0.52	912.30	14.50	12.85
Cosmos [47]	49.42	29.77	0.70	0.26	448.12	6.40	18.73
HunyuanVideo [33]	53.54	29.43	0.71	0.26	384.31	6.10	18.88
WAN2.2 [64]	53.99	35.69	0.72	0.23	322.17	5.78	20.44
EgoForge (Ours)	61.25	39.30	0.79	0.15	182.25	2.83	24.08

evaluation covering all interaction categories in our taxonomy. Details about the annotation pipeline and dataset statistics are provided in Appendix C.

Evaluation Metrics. We employ a suite of metrics that capture complementary aspects of visual and temporal quality to comprehensively evaluate performance on X-Ego. We measure low-level visual fidelity using PSNR [29] and SSIM [70]. To assess perceptual alignment, we employ LPIPS [85], DINO-Score [82] and CLIP-Score [53], which captures higher-level semantic correspondence. We further measure distributional realism using FVD [55]. Finally, we measure temporal and motion fidelity by computing the Mean Squared Error (MSE) between optical flow fields. More details are provided in Appendix D.

Implementation Details. EgoForge utilizes the Wan2.2-5B [64] model as the base generator. We employ a two-stage training process. The first stage is Denoising Fine-Tuning (FT), where we fine-tune the model on 13,000 data samples. In this stage, we freeze the DINOv3 and VGGT backbones. The second stage is VideoDiffusionNFT, for which we use 2,000 data samples for training. During this stage, only the diffusion model itself is trained, while all other components are frozen. We fine-tune the model using Low-Rank Adaptation (LoRA) with a rank of 32, optimized with Adam at a learning rate of $1e^{-4}$ under mixed-precision (bf16) training. The core training stage runs for 10 epochs on 8 H100 GPUs, requiring approximately 108 hours. We train with a batch size of 1 at a resolution of 720p, processing input videos at 24 fps and using 241 frames per sequence. During reward acquisition, we generate 6 video variations per sample (batch size 1) to obtain diverse trajectories and corresponding reward signals.

4.2. Experimental Results

Quantitative comparisons. We compare EgoForge with state-of-the-art general-purpose video models, including Cosmos [47], HunyuanVideo [33], and WAN2.2 [64], as well as egocentric-specific models such as EgoDreamer [67] and Handi [36]. These models represent the strongest available general-purpose video generators and the most relevant publicly available egocentric baselines. To ensure a fair evaluation, we fine-tune video models on our X-Ego dataset to bridge the domain gap.

As shown in Table 3, **EgoForge** consistently outperforms all baselines across all metrics. Compared with the strongest baseline, it improves semantic alignment by +13.5% DINO-Score and +10.1% CLIP-Score, while increasing structural fidelity (+9.7% SSIM) and reconstruction quality (+17.8% PSNR). At the same time, perceptual error is substantially reduced (35% lower LPIPS). Most notably, EgoForge achieves large gains in temporal modeling, reducing FVD by 43% and flow MSE by 51%, indicating significantly more coherent motion and stable scene dynamics. These improvements demonstrate that EgoForge more effectively captures egocentric motion patterns than baselines.

To ensure a fair and rigorous comparison, we further enhance the baseline models using three progressive

Table 5: Ablation on EgoForge modules. We evaluate the impact of diffusion finetuning (FT), geometry weak supervision (GWS), and the proposed VideoDiffusionNFT refinement. Each component consistently improves performance across semantic, perceptual, and temporal metrics, with the full EgoForge model achieving the best overall results.

FT	GWS	VideoDiffusionNFT	DINO-Score↑	CLIP-Score↑	SSIM↑	LPIPS↓	FVD↓	flow MSE↓	PSNR↑
✓	✗	✗	56.81	37.10	0.74	0.21	260.89	4.82	21.92
✓	✓	✗	58.92	38.05	0.76	0.18	218.72	3.92	22.87
✓	✓	✓	61.25	39.30	0.79	0.15	182.25	2.83	24.08

strategies: naive visual augmentation (+EV), text-only domain adaptation (+TT), and our structured conditioning injection with Geometry Weak Supervision (+CI). As shown in Table 2, while these enhancements significantly boost the performance of general models, our EgoForge model still achieves the best results across all seven metrics. Specifically, it reaches a state-of-the-art FVD of 182.25 and flow MSE of 2.83. These results demonstrate that even when provided with similar geometric priors (+CI), EgoForge’s specialized architecture is inherently more effective at capturing the unique dynamics and temporal consistency required for egocentric video synthesis.

User study. We conduct a comprehensive human evaluation study, with the comparative results detailed in Table 4. We recruit 20 annotators to evaluate 25 groups of videos, where each group contains outputs from all competing methods paired with the corresponding text prompt. Participants were provided with a detailed annotation protocol to rate each video on a 1-to-5 scale across five dimensions: Quality (overall visual coherence), Fidelity (identity preservation and absence of artifacts or distortions), Smooth Motion (temporal consistency and fluidity of subject movement), Smooth Environment (background stability and smoothness), and Alignment (semantic correspondence between video and input). Our method achieves substantial gains in Alignment (4.75) and Fidelity (4.71), surpassing the strongest competitors (*e.g.*, +1.60 in Alignment over WAN2.2). These results, combined with superior scores in temporal and environmental smoothness, validate the effectiveness of our approach in generating high-quality, prompt-aligned videos.

Table 4: User study. We measure “Q.” Quality (synthesis quality), “F.” Fidelity (object identity preservation), “M.” Smooth Motion (motion consistency), “E.” Smooth Environment (background environment consistency), and “A.” Alignment with the input conditioning. Each metric is rated from 1 (worst) to 5 (best). *Best model variants from Table 2.

Model	Q.↑	F.↑	M.↑	E.↑	A.↑
Cosmos* [47]	3.29	2.54	3.07	2.47	2.19
Hunyuan* [33]	3.46	2.86	3.72	3.16	3.08
WAN2.2* [64]	3.22	3.48	3.82	4.07	3.15
EgoForge (Ours)	4.58	4.71	4.25	4.48	4.75

4.3. Ablations

Effectiveness of VideoDiffusionNFT. We first evaluate the contribution of our proposed trajectory-level reward-guided refinement. We compare a baseline model trained with only supervised denoising finetuning (+ Denoising FT) against a variant that also incorporates the VideoDiffusionNFT optimization. As shown in Table 5, the model without VideoDiffusionNFT exhibits weaker alignment and reduced temporal coherence. In contrast, training with VideoDiffusionNFT yields the largest gains across all metrics, with clear improvements in generation quality and temporal consistency, demonstrating the value of VideoDiffusionNFT.

Effect of Geometric Alignment Loss. We analyze the impact of geometric alignment. We compare our full model, which includes this loss, against the variant trained only with denoising finetuning and

Table 6: Effect of reward components in VideoDiffusionNFT. Each reward term contributes to improved semantic alignment and temporal coherence, while the full reward composition yields the strongest performance across all metrics.

Rewards	DINO-Score \uparrow	CLIP-Score \uparrow	SSIM \uparrow	LPIPS \downarrow	FVD \downarrow	flow MSE \downarrow	PSNR \uparrow
\times $\mathcal{R}_{\text{goal}}$	59.62	38.49	0.78	0.16	205.96	3.48	23.48
\times \mathcal{R}_{env}	60.67	39.05	0.78	0.16	200.49	3.43	23.60
\times $\mathcal{R}_{\text{temp}}$	60.78	39.11	0.78	0.16	213.25	3.70	23.72
\times \mathcal{R}_{per}	60.32	38.80	0.77	0.18	204.13	3.48	23.17
EgoForge (Ours)	61.25	39.30	0.79	0.15	182.25	2.83	24.08

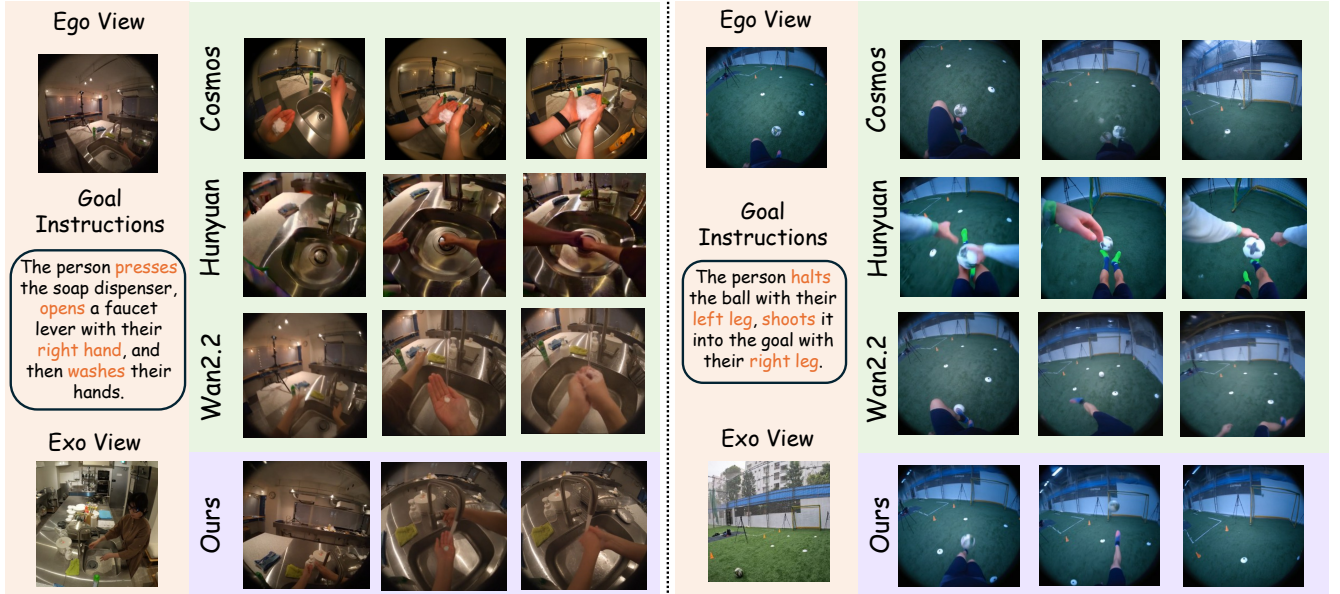


Figure 3: Qualitative Comparison between EgoForge and baselines. Sample frames from generated videos illustrating two scenarios. Top row: In the hand-washing task, baselines struggle with object consistency (e.g., Cosmos hallucinates the soap source) or ignore scene context (e.g., Wan2.2 bypasses the on-table soap), while Ours successfully executes the action using existing objects. Bottom row: In the soccer task, baselines exhibit severe artifacts like ghosting (Cosmos) or fail to follow precise instructions regarding motion and goals (Hunyuan, Wan2.2). EgoForge accurately executes the complex command: trapping with the left leg and shooting with the right.

VideoDiffusionNFT but without geometric supervision. As shown in Table 5, geometric alignment substantially enhances spatial structure and realism, increasing DINO-Score by +2.1 and CLIP-Score by +1.9, while reducing LPIPS to 0.16 and improving flow MSE to 3.92. Removing this loss results in a noticeable drop in performance, with the model struggling to preserve geometric consistency and realism. These results confirm that enforcing geometry-level coordination is essential for accurate, stable, and physically grounded world simulations.

Ablation Study on Rewards. Table 6 evaluates the contribution of each reward component ($\mathcal{R}_{\text{goal}}$, \mathcal{R}_{env} , $\mathcal{R}_{\text{temp}}$, \mathcal{R}_{per}) in EgoForge. Our results demonstrate that all terms are essential for high-quality egocentric simulation. Specifically, removing \mathcal{R}_{per} leads to the sharpest decline in visual metrics (SSIM, PSNR, LPIPS). $\mathcal{R}_{\text{temp}}$ is critical for temporal consistency; its absence causes the most significant degradation in FVD and flow MSE. $\mathcal{R}_{\text{goal}}$ primarily ensures semantic and task alignment, as evidenced by the largest drops in CLIP and

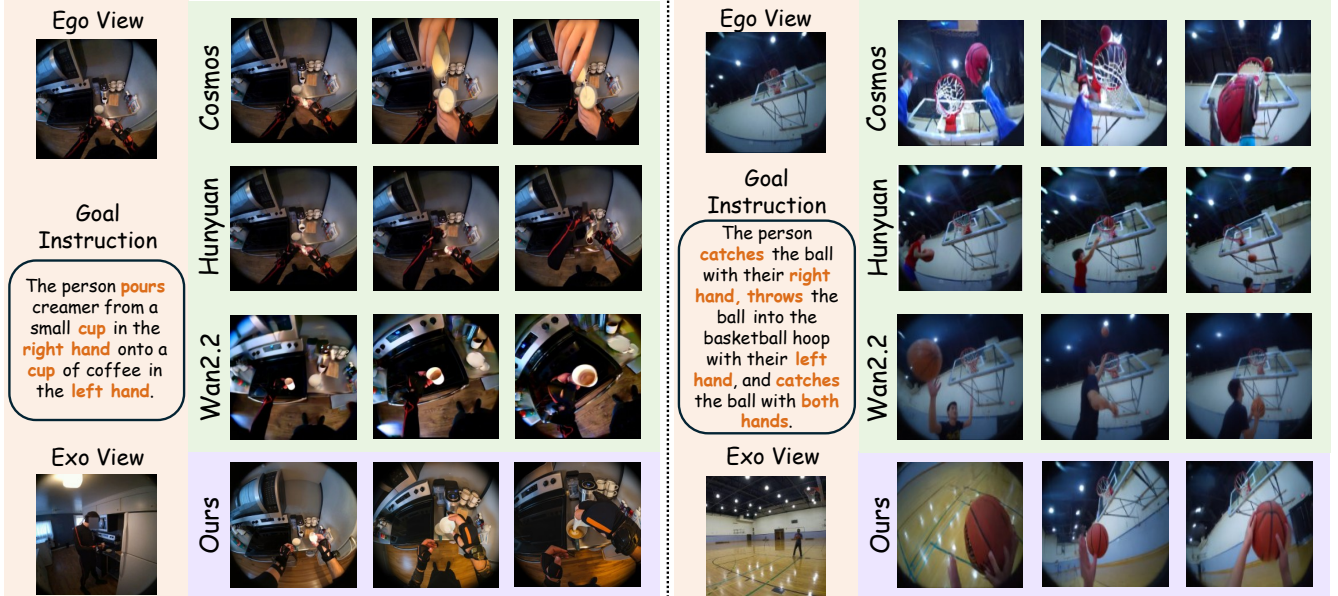


Figure 4: Qualitative Comparison between EgoForge and baselines. EgoForge accurately reconstructs multi-step, causally ordered actions, preserving hand–object geometry, temporal consistency, and goal alignment. For instance, in the first example, Cosmos erroneously generates a third hand, Hunyuan depicts a disconnected arm, and Wan2.2 fails to complete the coffee-pouring task. In the second example, Cosmos generates multiple balls, while both Hunyuan and Wan2.2 generate an incorrect person to perform the action. In contrast, EgoForge accurately completes both tasks.

DINO scores without it. Finally, omitting \mathcal{R}_{env} results in moderate performance across all metrics, reflecting its role in background consistency and physical plausibility.

4.4. Qualitative Analysis

Figure 4 and Figure 3 provide qualitative comparisons of our model, EgoForge, against the Cosmos [1], Hunyuan [33], and Wan2.2 [64] baselines for two complex, long-horizon egocentric tasks. Results demonstrate that EgoForge generates significantly more physically plausible and temporally coherent video sequences. Other baseline models suffer from generating only from an egocentric view, failing to maintain the egocentric perspective, distorting the objects, or producing physically implausible action sequences.

Moreover, Figure 5 visualizes EgoForge’s video quality by displaying dense frame sequences demonstrating coherent dynamics. Across diverse activities and environments, the generated rollouts follow the specified instructions while maintaining stable scene structure and consistent egocentric viewpoint motion. Importantly, complex multi-step behaviors (*e.g.*, manipulating objects, interacting with appliances, or performing physical activities) unfold naturally over time, demonstrating that EgoForge captures both the procedural structure of actions and the surrounding scene context required for goal-directed egocentric simulation. Additional visualization examples can be found in Appendix E.

Finally, Figure 6 provides a qualitative comparison of EgoForge’s generation with and without an auxiliary exocentric view image. Results show that EgoForge generates plausible egocentric rollouts using instruction guidance alone (Rows 1 & 3), while incorporating an auxiliary exocentric image further improves spatial grounding and scene consistency by anchoring the simulation to the reference environment (Rows 2 & 4),

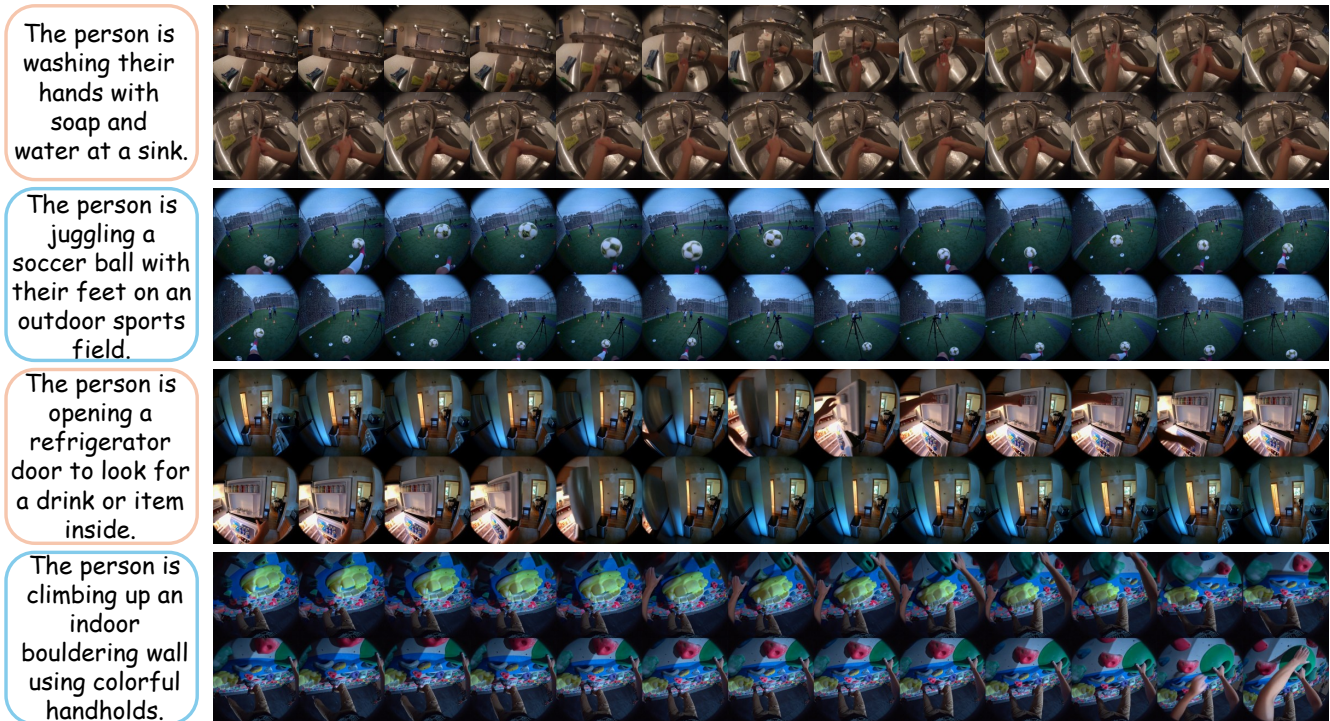


Figure 5: Qualitative egocentric video rollouts. EgoForge generates temporally coherent first-person video trajectories that follow the intended activity while preserving scene structure and realistic hand–object interactions across diverse environments. We provide dense frame sequences to visualize our video result.

such as the *potted plants on the windowsill* and the distinctive *red and green rubberized surface* of the court. This confirms that an exo-view frame can act as effective guidance that EgoForge can accurately inject into the simulated trajectory.

4.5. Real-world Smart-Glasses Experiment

Previous egocentric world models have typically been tested only with in-domain data, ignoring the complexity of real-world out-of-domain (OOD) data. To fill this gap, we deploy EgoForge in a real-world environment using ARGO smartglasses for the first time. The selected tasks are shown in Figure 1 and include diverse multi-step actions such as “Pour into the cup...put the can back”, “Jump to the pool ...arms forward”, “Take a marker... draw a circle”, and “Take a bottle of water ...on the box”. For each task, a single egocentric frame is captured directly from the smartglasses, while an auxiliary exo-view from another participant’s reference image is provided alongside the text-action guidance. The resulting *Simulated Videos* (Fig 1, right) show that EgoForge can reliably transfer exocentric cues and follow high-level semantic intent, producing coherent, controllable rollouts despite significant real-world variability. Device details available in Appendix F.

5. Conclusion

We introduce EgoForge, a goal-directed egocentric world simulator capable of generating coherent first-person video rollouts from minimal visual context. By conditioning generation on an egocentric observation, high-level instruction, and optional exocentric reference, EgoForge models how scenes evolve as users perform goal-oriented actions. Our framework combines geometry-aware grounding to improve spatial consistency



Figure 6: Qualitative comparison of EgoForge with vs. without exocentric input. We compare EgoForge simulations generated from a text prompt alone (Rows 1 & 3, "Without Exo-View") against rollouts generated by combining the text prompt with a guiding auxiliary exocentric image (Rows 2 & 4, "With Exo-View"). As shown, EgoForge can be successfully steered toward simulations that inherit key semantic and stylistic properties from the reference exo-view image. For instance, the kitchen scene (Row 2) correctly incorporates the *potted plants on the windowsill* from the reference image, and the basketball court scene (Row 4) adopts the *red and green rubberized surface* from its corresponding exo-view image.

with VideoDiffusionNFT, a novel trajectory-level reward-guided refinement method that balances goal completion, scene stability, temporal causality, and perceptual fidelity during diffusion sampling. Extensive experiments and validation on smart-glasses scenarios demonstrate that EgoForge consistently outperforms strong baselines across metrics, producing egocentric rollouts with improved instruction alignment, realistic egocentric motion, and stable scene evolution. We hope this direction will facilitate future research on immersive world models, interactive simulation, and human-centered XR systems.

References

- [1] Niket Agarwal, Arslan Ali, Maciej Bala, Yogesh Balaji, Erik Barker, Tiffany Cai, Prithvijit Chattopadhyay, Yongxin Chen, Yin Cui, Yifan Ding, et al. Cosmos world foundation model platform for physical ai. *arXiv preprint arXiv:2501.03575*, 2025.
- [2] Eloi Alonso, Adam Jelley, Vincent Micheli, Anssi Kanervisto, Amos J Storkey, Tim Pearce, and François Fleuret. Diffusion for world modeling: Visual details matter in atari. *Advances in Neural Information Processing Systems (NeurIPS)*, pages 58757–58791, 2024.
- [3] Kumar Ashutosh, Rohit Girdhar, Lorenzo Torresani, and Kristen Grauman. Hiervl: Learning hierarchical video-language embeddings. In *IEEE Conference on Computer Vision and Pattern Recognition (CVPR)*, pages 23066–23078, 2023.

-
- [4] Philip J. Ball, Jakob Bauer, Frank Belletti, Bethanie Brownfield, Ariel Ephrat, Shlomi Fruchter, Agrim Gupta, et al. Genie 3: A new frontier for world models. 2025.
- [5] Amir Bar, Gaoyue Zhou, Danny Tran, Trevor Darrell, and Yann LeCun. Navigation world models. In *IEEE Conference on Computer Vision and Pattern Recognition (CVPR)*, pages 15791–15801, 2025.
- [6] Andreas Blattmann, Tim Dockhorn, Sumith Kulal, Daniel Mendeleevitch, Maciej Kilian, Dominik Lorenz, Yam Levi, Zion English, Vikram Voleti, Adam Letts, et al. Stable video diffusion: Scaling latent video diffusion models to large datasets. *arXiv preprint arXiv:2311.15127*, 2023.
- [7] Jake Bruce, Michael D Dennis, Ashley Edwards, Jack Parker-Holder, Yuge Shi, Edward Hughes, Matthew Lai, Aditi Mavalankar, Richie Steigerwald, Chris Apps, Yusuf Aytar, Sarah Maria Elisabeth Bechtler, Feryal Behbahani, Stephanie C.Y. Chan, Nicolas Heess, Lucy Gonzalez, Simon Osindero, Sherjil Ozair, Scott Reed, Jingwei Zhang, Konrad Zolna, Jeff Clune, Nando de Freitas, Satinder Singh, and Tim Rocktäschel. Genie: Generative interactive environments. In *International Conference on Machine Learning (ICML)*, 2024.
- [8] Xu Cao, Yifan Shen, Bolin Lai, Wenqian Ye, Yunsheng Ma, Joerg Heintz, Jintai Chen, Meihuan Huang, Jianguo Cao, Aidong Zhang, et al. What is the visual cognition gap between humans and multimodal llms? *arXiv preprint arXiv:2406.10424*, 2024.
- [9] Haoxuan Che, Xuanhua He, Quande Liu, Cheng Jin, and Hao Chen. Gamegen-x: Interactive open-world game video generation. In *International Conference on Learning Representations (ICLR)*, 2025.
- [10] Haoxin Chen, Menghan Xia, Yingqing He, Yong Zhang, Xiaodong Cun, Shaoshu Yang, Jinbo Xing, Yaofang Liu, Qifeng Chen, Xintao Wang, et al. Videocrafter1: Open diffusion models for high-quality video generation. *arXiv preprint arXiv:2310.19512*, 2023.
- [11] Haoxin Chen, Yong Zhang, Xiaodong Cun, Menghan Xia, Xintao Wang, Chao Weng, and Ying Shan. Videocrafter2: Overcoming data limitations for high-quality video diffusion models. In *IEEE Conference on Computer Vision and Pattern Recognition (CVPR)*, pages 7310–7320, 2024.
- [12] Junsong Chen, Jincheng YU, Chongjian GE, Lewei Yao, Enze Xie, Zhongdao Wang, James Kwok, Ping Luo, Huchuan Lu, and Zhenguo Li. Pixart- α : Fast training of diffusion transformer for photorealistic text-to-image synthesis. In *International Conference on Learning Representations (ICLR)*, 2024.
- [13] Feng Cheng, Mi Luo, Huiyu Wang, Alex Dimakis, Lorenzo Torresani, Gedas Bertasius, and Kristen Grauman. 4diff: 3d-aware diffusion model for third-to-first viewpoint translation. In *European Conference on Computer Vision (ECCV)*, 2024.
- [14] Nicola Dainese, Matteo Merler, Minttu Alakuijala, and Pekka Marttinen. Generating code world models with large language models guided by monte carlo tree search. *Advances in Neural Information Processing Systems (NeurIPS)*, 37:60429–60474, 2024.
- [15] Dima Damen, Hazel Doughty, Giovanni Maria Farinella, Sanja Fidler, Antonino Furnari, Evangelos Kazakos, Davide Moltisanti, Jonathan Munro, Toby Perrett, Will Price, et al. Scaling egocentric vision: The epic-kitchens dataset. In *European Conference on Computer Vision (ECCV)*, pages 720–736, 2018.
- [16] Dima Damen, Hazel Doughty, Giovanni Maria Farinella, Sanja Fidler, Antonino Furnari, Evangelos Kazakos, Davide Moltisanti, Jonathan Munro, Toby Perrett, Will Price, et al. The epic-kitchens dataset:
-

-
- Collection, challenges and baselines. *IEEE Transactions on Pattern Analysis and Machine Intelligence*, 43(11):4125–4141, 2020.
- [17] Dima Damen, Hazel Doughty, Giovanni Maria Farinella, Antonino Furnari, Evangelos Kazakos, Jian Ma, Davide Moltisanti, Jonathan Munro, Toby Perrett, Will Price, et al. Rescaling egocentric vision: Collection, pipeline and challenges for epic-kitchens-100. *International Journal on Computer Vision (IJCV)*, 130(1):33–55, 2022.
- [18] Aurèle Hainaut Werner Duvaud and Aurèle Hainaut. Muzero general: Open reimplement of muzero. <https://github.com/werner-duvaud/muzero-general>, 2019.
- [19] Ignat Georgiev, Varun Giridhar, Nicklas Hansen, and Animesh Garg. PWM: Policy learning with multi-task world models. In *International Conference on Learning Representations (ICLR)*, 2025.
- [20] Andrey Gorodetskiy, Konstantin Mironov, and Aleksandr Panov. Model-based policy optimization using symbolic world model. In *International Conference on Intelligent Robots and Systems (IROS)*, pages 664–669, 2024.
- [21] Kristen Grauman, Andrew Westbury, Eugene Byrne, Zachary Chavis, Antonino Furnari, Rohit Girdhar, Jackson Hamburger, Hao Jiang, Miao Liu, Xingyu Liu, et al. Ego4d: Around the world in 3,000 hours of egocentric video. In *IEEE Conference on Computer Vision and Pattern Recognition (CVPR)*, pages 18995–19012, 2022.
- [22] Kristen Grauman, Andrew Westbury, Lorenzo Torresani, Kris Kitani, Jitendra Malik, Triantafyllos Afouras, Kumar Ashutosh, Vijay Baiyya, Siddhant Bansal, Bikram Boote, et al. Ego-exo4d: Understanding skilled human activity from first-and third-person perspectives. In *IEEE Conference on Computer Vision and Pattern Recognition (CVPR)*, pages 19383–19400, 2024.
- [23] Danijar Hafner, Timothy Lillicrap, Ian Fischer, Ruben Villegas, David Ha, Honglak Lee, and James Davidson. Learning latent dynamics for planning from pixels. In *International Conference on Machine Learning (ICML)*, pages 2555–2565, 2019.
- [24] Danijar Hafner, Timothy Lillicrap, Jimmy Ba, and Mohammad Norouzi. Dream to control: Learning behaviors by latent imagination. In *International Conference on Learning Representations (ICLR)*, 2020.
- [25] Nicklas Hansen, Hao Su, and Xiaolong Wang. Td-mpc2: Scalable, robust world models for continuous control. In *International Conference on Learning Representations (ICLR)*, 2024.
- [26] Jonathan Ho, Ajay Jain, and Pieter Abbeel. Denoising diffusion probabilistic models. *Advances in Neural Information Processing Systems (NeurIPS)*, 33:6840–6851, 2020.
- [27] Anthony Hu, Lloyd Russell, Hudson Yeo, Zak Murez, George Fedoseev, Alex Kendall, Jamie Shotton, and Gianluca Corrado. Gaia-1: A generative world model for autonomous driving. *arXiv preprint arXiv:2309.17080*, 2023.
- [28] Yifei Huang, Minjie Cai, Zhenqiang Li, and Yoichi Sato. Predicting gaze in egocentric video by learning task-dependent attention transition. In *European Conference on Computer Vision (ECCV)*, pages 754–769, 2018.
- [29] Quan Huynh-Thu and Mohammed Ghanbari. Scope of validity of psnr in image/video quality assessment. *Electronics letters*, 44(13):800–801, 2008.
-

-
- [30] Wenqi Jia, Miao Liu, and James M Rehg. Generative adversarial network for future hand segmentation from egocentric video. In *European Conference on Computer Vision (ECCV)*, pages 639–656, 2022.
- [31] Taewoong Kang, Kinam Kim, Dohyeon Kim, Minhoo Park, Junha Hyung, and Jaegul Choo. Egox: Egocentric video generation from a single exocentric video. *arXiv preprint arXiv:2512.08269*, 2025.
- [32] Evangelos Kazakos, Arsha Nagrani, Andrew Zisserman, and Dima Damen. Epic-fusion: Audio-visual temporal binding for egocentric action recognition. In *International Conference on Computer Vision (ICCV)*, pages 5492–5501, 2019.
- [33] Weijie Kong, Qi Tian, Zijian Zhang, Rox Min, Zuozhuo Dai, Jin Zhou, Jiangfeng Xiong, Xin Li, Bo Wu, Jianwei Zhang, et al. Hunyuanvideo: A systematic framework for large video generative models. *arXiv preprint arXiv:2412.03603*, 2024.
- [34] Jiaman Li, Karen Liu, and Jiajun Wu. Ego-body pose estimation via ego-head pose estimation. In *IEEE Conference on Computer Vision and Pattern Recognition (CVPR)*, pages 17142–17151, 2023.
- [35] Qifeng Li, Xiaosong Jia, Shaobo Wang, and Junchi Yan. Think2drive: Efficient reinforcement learning by thinking with latent world model for autonomous driving (in carla-v2). In *European Conference on Computer Vision (ECCV)*, pages 142–158, 2024.
- [36] Yayuan Li, Zhi Cao, and Jason J Corso. Handi: Hand-centric text-and-image conditioned video generation. *arXiv preprint arXiv:2412.04189*, 2024.
- [37] Bin Lin, Yunyang Ge, Xinhua Cheng, Zongjian Li, Bin Zhu, Shaodong Wang, Xianyi He, Yang Ye, Shenghai Yuan, Liuhan Chen, et al. Open-sora plan: Open-source large video generation model. *arXiv preprint arXiv:2412.00131*, 2024.
- [38] Jessy Lin, Yuqing Du, Olivia Watkins, Danijar Hafner, Pieter Abbeel, Dan Klein, and Anca Dragan. Learning to model the world with language. In *International Conference on Machine Learning (ICML)*, 2024.
- [39] Kevin Qinghong Lin, Jinpeng Wang, Mattia Soldan, Michael Wray, Rui Yan, Eric Z Xu, Difei Gao, Rong-Cheng Tu, Wenzhe Zhao, Weijie Kong, et al. Egocentric video-language pretraining. *Advances in Neural Information Processing Systems (NeurIPS)*, 35:7575–7586, 2022.
- [40] Yaron Lipman, Ricky TQ Chen, Heli Ben-Hamu, Maximilian Nickel, and Matt Le. Flow matching for generative modeling. *arXiv preprint arXiv:2210.02747*, 2022.
- [41] Jia-Wei Liu, Weijia Mao, Zhongcong Xu, Jussi Keppo, and Mike Zheng Shou. Exocentric-to-egocentric video generation. In *Advances in Neural Information Processing Systems (NeurIPS)*, 2024.
- [42] Shaowei Liu, Subarna Tripathi, Somdeb Majumdar, and Xiaolong Wang. Joint hand motion and interaction hotspots prediction from egocentric videos. In *IEEE Conference on Computer Vision and Pattern Recognition (CVPR)*, pages 3282–3292, 2022.
- [43] Yuanzhe Liu, Jingyuan Zhu, Yuchen Mo, Gen Li, Xu Cao, Jin Jin, Yifan Shen, Zhengyuan Li, Tianjiao Yu, Wenzhen Yuan, et al. Palm: Progress-aware policy learning via affordance reasoning for long-horizon robotic manipulation. *arXiv preprint arXiv:2601.07060*, 2026.
- [44] Zhengyi Luo, Ryo Hachiuma, Ye Yuan, and Kris Kitani. Dynamics-regulated kinematic policy for egocentric pose estimation. *Advances in Neural Information Processing Systems (NeurIPS)*, 34:25019–25032, 2021.
-

-
- [45] Lingni Ma, Yuting Ye, Fangzhou Hong, Vladimir Guzov, Yifeng Jiang, Rowan Postyeni, Luis Pesqueira, Alexander Gamino, Vijay Baiyya, Hyo Jin Kim, et al. Nymeria: A massive collection of multimodal egocentric daily motion in the wild. In *European Conference on Computer Vision (ECCV)*, pages 445–465, 2024.
- [46] Yutaka Matsuo, Yann LeCun, Maneesh Sahani, Doina Precup, David Silver, Masashi Sugiyama, Eiji Uchibe, and Jun Morimoto. Deep learning, reinforcement learning, and world models. *Neural Networks*, 152:267–275, 2022.
- [47] NVIDIA, Arslan Ali, Junjie Bai, Maciej Bala, Yogesh Balaji, Aaron Blakeman, Tiffany Cai, Jiaxin Cao, Tianshi Cao, Elizabeth Cha, Yu-Wei Chao, et al. World simulation with video foundation models for physical ai, 2025.
- [48] OpenAI. Creating video from text. In <https://openai.com/index/sora/>, 2024.
- [49] Junho Park, Andrew Sangwoo Ye, and Taein Kwon. Egoworld: Translating exocentric view to egocentric view using rich exocentric observations. *arXiv preprint arXiv:2506.17896*, 2025.
- [50] William Peebles and Saining Xie. Scalable diffusion models with transformers. In *International Conference on Computer Vision (ICCV)*, pages 4195–4205, 2023.
- [51] Dustin Podell, Zion English, Kyle Lacey, Andreas Blattmann, Tim Dockhorn, Jonas Müller, Joe Penna, and Robin Rombach. SDXL: Improving latent diffusion models for high-resolution image synthesis. In *International Conference on Learning Representations (ICLR)*, 2024.
- [52] Shraman Pramanick, Yale Song, Sayan Nag, Kevin Qinghong Lin, Hardik Shah, Mike Zheng Shou, Rama Chellappa, and Pengchuan Zhang. Egovlpv2: Egocentric video-language pre-training with fusion in the backbone. In *International Conference on Computer Vision (ICCV)*, pages 5285–5297, 2023.
- [53] Alec Radford, Jong Wook Kim, Chris Hallacy, Aditya Ramesh, Gabriel Goh, Sandhini Agarwal, Girish Sastry, Amanda Askell, Pamela Mishkin, Jack Clark, et al. Learning transferable visual models from natural language supervision. In *International Conference on Machine Learning (ICML)*, 2021.
- [54] Francesco Ragusa, Giovanni Maria Farinella, and Antonino Furnari. Stillfast: An end-to-end approach for short-term object interaction anticipation. In *IEEE Conference on Computer Vision and Pattern Recognition (CVPR)*, pages 3636–3645, 2023.
- [55] Ruslan Rakhimov, Denis Volkhonskiy, Alexey Artemov, Denis Zorin, and Evgeny Burnaev. Latent video transformer. *arXiv preprint arXiv:2006.10704*, 2020.
- [56] Robin Rombach, Andreas Blattmann, Dominik Lorenz, Patrick Esser, and Björn Ommer. High-resolution image synthesis with latent diffusion models. In *IEEE Conference on Computer Vision and Pattern Recognition (CVPR)*, pages 10684–10695, 2022.
- [57] Lloyd Russell, Anthony Hu, Lorenzo Bertoni, George Fedoseev, Jamie Shotton, Elahe Arani, and Gianluca Corrado. Gaia-2: A controllable multi-view generative world model for autonomous driving. *arXiv preprint arXiv:2503.20523*, 2025.
- [58] Yifan Shen, Yuanzhe Liu, Jingyuan Zhu, Xu Cao, Xiaofeng Zhang, Yixiao He, Wenming Ye, James Matthew Rehg, and Ismini Lourentzou. Fine-grained preference optimization improves spatial reasoning in vlms. *arXiv preprint arXiv:2506.21656*, 2025.
-

-
- [59] Yang Song and Stefano Ermon. Generative modeling by estimating gradients of the data distribution. *Advances in Neural Information Processing Systems (NeurIPS)*, 32, 2019.
- [60] Yang Song, Jascha Sohl-Dickstein, Diederik P Kingma, Abhishek Kumar, Stefano Ermon, and Ben Poole. Score-based generative modeling through stochastic differential equations. In *International Conference on Learning Representations (ICLR)*, 2021.
- [61] Ruixiang Sun, Hongyu Zang, Xin Li, and Riashat Islam. Learning latent dynamic robust representations for world models. In *International Conference on Machine Learning (ICML)*, pages 47234–47260, 2024.
- [62] Yuanpeng Tu, Hao Luo, Xi Chen, Xiang Bai, Fan Wang, and Hengshuang Zhao. Playerone: Egocentric world simulator. In *Advances in Neural Information Processing Systems (NeurIPS)*, 2025.
- [63] Dani Valevski, Yaniv Leviathan, Moab Arar, and Shlomi Fruchter. Diffusion models are real-time game engines. In *International Conference on Learning Representations (ICLR)*, 2025.
- [64] Team Wan, Ang Wang, Baole Ai, Bin Wen, Chaojie Mao, Chen-Wei Xie, Di Chen, Feiwu Yu, Haiming Zhao, Jianxiao Yang, Jianyuan Zeng, Jiayu Wang, et al. Wan: Open and advanced large-scale video generative models. *arXiv preprint arXiv:2503.20314*, 2025.
- [65] Jian Wang, Diogo Luvizon, Weipeng Xu, Lingjie Liu, Kripasindhu Sarkar, and Christian Theobalt. Scene-aware egocentric 3d human pose estimation. In *IEEE Conference on Computer Vision and Pattern Recognition (CVPR)*, pages 13031–13040, 2023.
- [66] Jianyuan Wang, Minghao Chen, Nikita Karaev, Andrea Vedaldi, Christian Rupprecht, and David Novotny. Vggt: Visual geometry grounded transformer. *arXiv preprint arXiv:2503.11651*, 2025.
- [67] Xiaofeng Wang, Kang Zhao, Feng Liu, Jiayu Wang, Guosheng Zhao, Xiaoyi Bao, Zheng Zhu, Yingya Zhang, and Xingang Wang. Egovid-5m: A large-scale video-action dataset for egocentric video generation. *arXiv preprint arXiv:2411.08380*, 2024.
- [68] Xiaohan Wang, Linchao Zhu, Heng Wang, and Yi Yang. Interactive prototype learning for egocentric action recognition. In *International Conference on Computer Vision (ICCV)*, pages 8168–8177, 2021.
- [69] Zhizun Wang and David Meger. Leveraging world model disentanglement in value-based multi-agent reinforcement learning. In *International Joint Conference on Neural Networks (IJCNN)*, pages 1–10. IEEE, 2025.
- [70] Zhou Wang, Alan C Bovik, Hamid R Sheikh, and Eero P Simoncelli. Image quality assessment: from error visibility to structural similarity. *IEEE Transactions on Image Processing*, 13(4):600–612, 2004.
- [71] Haoyu Wu, Diankun Wu, Tianyu He, Junliang Guo, Yang Ye, Yueqi Duan, and Jiang Bian. Geometry forcing: Marrying video diffusion and 3d representation for consistent world modeling. *arXiv preprint arXiv:2507.07982*, 2025.
- [72] Philipp Wu, Alejandro Escontrela, Danijar Hafner, Pieter Abbeel, and Ken Goldberg. Daydreamer: World models for physical robot learning. In *Conference on Robot Learning (CoRL)*, 2023.
- [73] Enze Xie, Junsong Chen, Junyu Chen, Han Cai, Haotian Tang, Yujun Lin, Zhekai Zhang, Muyang Li, Ligeng Zhu, Yao Lu, et al. Sana: Efficient high-resolution image synthesis with linear diffusion transformers. *arXiv preprint arXiv:2410.10629*, 2024.
-

-
- [74] Jingqiao Xiu, Fangzhou Hong, Yicong Li, Mengze Li, Wentao Wang, Sirui Han, Liang Pan, and Ziwei Liu. Egotwin: Dreaming body and view in first person. *arXiv preprint arXiv:2508.13013*, 2025.
- [75] Jilan Xu, Yifei Huang, Baoqi Pei, Junlin Hou, Qingqiu Li, Guo Chen, Yuejie Zhang, Rui Feng, and Weidi Xie. Egoexo-gen: Ego-centric video prediction by watching exo-centric videos. *arXiv preprint arXiv:2504.11732*, 2025.
- [76] Bufang Yang, Lilin Xu, Liekang Zeng, Kaiwei Liu, Siyang Jiang, Wenrui Lu, Hongkai Chen, Xiaofan Jiang, Guoliang Xing, and Zhenyu Yan. Contextagent: Context-aware proactive llm agents with open-world sensory perceptions. *arXiv preprint arXiv:2505.14668*, 2025.
- [77] Sherry Yang, Yilun Du, Seyed Ghasemipour, Jonathan Tompson, Leslie Kaelbling, Dale Schuurmans, and Pieter Abbeel. Learning interactive real-world simulators. In *International Conference on Learning Representations (ICLR)*, pages 45210–45234, 2024.
- [78] Yufei Ye, Xueting Li, Abhinav Gupta, Shalini De Mello, Stan Birchfield, Jiaming Song, Shubham Tulsiani, and Sifei Liu. Affordance diffusion: Synthesizing hand-object interactions. In *IEEE Conference on Computer Vision and Pattern Recognition (CVPR)*, pages 22479–22489, 2023.
- [79] Sihyun Yu, Sangkyung Kwak, Huiwon Jang, Jongheon Jeong, Jonathan Huang, Jinwoo Shin, and Saining Xie. Representation alignment for generation: Training diffusion transformers is easier than you think. *arXiv preprint arXiv:2410.06940*, 2025.
- [80] Tianjiao Yu, Xinzhuo Li, Yifan Shen, Yuanzhe Liu, and Ismini Lourentzou. Core3d: Collaborative reasoning as a foundation for 3d intelligence. *arXiv preprint arXiv:2512.12768*, 2025.
- [81] Binjie Zhang and Mike Zheng Shou. Ego-centric predictive model conditioned on hand trajectories. *arXiv preprint arXiv:2508.19852*, 2025.
- [82] Hao Zhang, Feng Li, Shilong Liu, Lei Zhang, Hang Su, Jun Zhu, Lionel M Ni, and Heung-Yeung Shum. Dino: Detr with improved denoising anchor boxes for end-to-end object detection. *arXiv preprint arXiv:2203.03605*, 2022.
- [83] Haoyu Zhang, Qiaohui Chu, Meng Liu, Haoxiang Shi, Yaowei Wang, and Liqiang Nie. Exo2ego: Exo-centric knowledge guided mllm for egocentric video understanding. *arXiv preprint arXiv:2503.09143*, 2025.
- [84] Mengmi Zhang, Keng Teck Ma, Joo Hwee Lim, Qi Zhao, and Jiashi Feng. Deep future gaze: Gaze anticipation on egocentric videos using adversarial networks. In *IEEE Conference on Computer Vision and Pattern Recognition (CVPR)*, pages 4372–4381, 2017.
- [85] Richard Zhang, Phillip Isola, Alexei A Efros, Eli Shechtman, and Oliver Wang. The unreasonable effectiveness of deep features as a perceptual metric. In *IEEE Conference on Computer Vision and Pattern Recognition (CVPR)*, 2018.
- [86] Yifan Zhang, Chunli Peng, Boyang Wang, Puyi Wang, Qingcheng Zhu, Fei Kang, Biao Jiang, Zedong Gao, Eric Li, Yang Liu, et al. Matrix-game: Interactive world foundation model. *arXiv preprint arXiv:2506.18701*, 2025.
- [87] Kaiwen Zheng, Huayu Chen, Haotian Ye, Haoxiang Wang, Qinsheng Zhang, Kai Jiang, Hang Su, Stefano Ermon, Jun Zhu, and Ming-Yu Liu. Diffusionnft: Online diffusion reinforcement with forward process. *arXiv preprint arXiv:2509.16117*, 2025.
-

- [88] Yunsong Zhou, Michael Simon, Zhenghao Peng, Sicheng Mo, Hongzi Zhu, Minyi Guo, and Bolei Zhou. Simgen: Simulator-conditioned driving scene generation. In *Advances in Neural Information Processing Systems (NeurIPS)*, volume 37, pages 48838–48874, 2024.
- [89] Haoyi Zhu, Yifan Wang, Jianjun Zhou, Wenzheng Chang, Yang Zhou, Zizun Li, Junyi Chen, Chunhua Shen, Jiangmiao Pang, and Tong He. Aether: Geometric-aware unified world modeling. In *International Conference on Computer Vision (ICCV)*, 2025.

A. More Information about VideoDiffusionNFT

In the main paper, we introduce VideoDiffusionNFT as a trajectory-level reinforcement stage to regulate the generation process on multiple, possibly conflicting conditioning signals. This appendix elaborates on why such an alignment is a non-trivial challenge, moving beyond standard per-frame conditioning. The difficulty arises from coordinating heterogeneous goals, semantic and visual, over entire, temporally-extended video rollouts. We highlight three specific complexities that necessitate a trajectory-level optimization approach.

Reward Sparsity and Temporal Credit Assignment. A primary challenge in egocentric simulation is that the criteria for success are often holistic and only measurable at an action sequence’s conclusion. For instance, our goal completion reward ($\mathcal{R}_{\text{goal}}$) evaluates whether a multi-step task (e.g., “put the can back”) was *ultimately* successful. This introduces a challenging temporal credit assignment problem. If a generated trajectory of T frames fails, it is non-trivial to pinpoint which of the T denoising steps, or which specific input mis-fusion at which timestep(s), contributed to the failure. Simple per-frame rewards (e.g., pixel-wise losses) cannot capture this procedural, long-horizon objective. Therefore, a reinforcement learning mechanism is required to optimize for this sparse, trajectory-wide reward, propagating the global success signal back to the entire generative process.

Preventing Goals Drift. In long-duration video synthesis, generative models are prone to “goals drift,” where the generated sequence gradually deviates from the initial conditioning signals. For example, while DiT blocks are conditioned on inputs at each step, there is no explicit mechanism in the standard diffusion objective to guarantee that a scene’s geometric structure or background elements (part of \mathcal{R}_{env}) remain consistent from frame 1 to frame T . Without a trajectory-level regularizer, the model might “forget” or “mutate” these goals, leading to artifacts such as a drifting environment or object flickering. VideoDiffusionNFT stage acts as this global supervisor, evaluating the entire rollout and penalizing sequences that exhibit such drift, thereby enforcing long-term temporal coherence.

The "Shortcut" Problem in Multimodal Fusion. As we note in the main paper, heterogeneous conditioning signals may dominate, conflict, or cancel out. A significant challenge is that the model can learn "shortcuts" to minimize the training loss without achieving genuine, collaborative fusion. For example, the model might find it easier to overfit to the auxiliary visual inputs, producing a stylistically similar video while entirely ignoring the complex procedural instructions in the text input. This results in a visually plausible rollout that fails the semantic task. Our multi-dimensional reward function (assessing goal, environment, causality, and fidelity) and the negative-aware finetuning structure directly combat this. By evaluating rollouts across multiple axes and explicitly repelling the model from “suboptimal” samples (e.g., low $\mathcal{R}_{\text{goal}}$ but high \mathcal{R}_{per}), VideoDiffusionNFT compels the model to find a policy that balances all inputs, disincentivizing shortcut solutions and enforcing true input collaboration.

B. VideoDiffusionNFT Reward Details

This appendix details reward design choices for our proposed VideoDiffusionNFT.

Goal Completion Reward ($\mathcal{R}_{\text{goal}}$). The goal completion reward ($\mathcal{R}_{\text{goal}}$) quantifies the overall success of the manipulation task by evaluating both the process and the final outcome. This 2.0-point metric is a composite function, $\mathcal{R}_{\text{goal}} = \mathcal{R}_{\text{task}} + \mathcal{R}_{\text{align}}$, where each component has a maximum value of 1.0. The Task Completion score ($\mathcal{R}_{\text{task}}$) assesses the dynamic fidelity of the video, rewarding the agentic world model for performing the necessary state changes and manipulations required to transition from the initial state to the final one. Concurrently, the Visual Alignment score ($\mathcal{R}_{\text{align}}$) evaluates the target outcome of the action by measuring

the semantic correspondence and spatial relationship of key elements between the video’s final frame and the target state image, ensuring the end state is verifiably correct.

Scene Consistency Reward (\mathcal{R}_{env}). To ensure the model focuses specifically on the manipulation task without altering the surrounding scene, we introduce the scene consistency reward (\mathcal{R}_{env}). This 2.0-point metric is critical for disentangling the required action from the background context, particularly when the target image exists in a different environment. It is defined as $\mathcal{R}_{\text{env}} = \mathcal{R}_{\text{consist}} + \mathcal{R}_{\text{contam}}$. The Consistency Score ($\mathcal{R}_{\text{consist}}$) measures the temporal stability of static environmental features between the initial state image and the entire video sequence, penalizing any unmotivated environmental drift. The Contamination Score ($\mathcal{R}_{\text{contam}}$) specifically penalizes the model for "hallucinating" or leaking environmental features (e.g., lighting, background objects, textures) that are present only in the target image but not in the initial state.

Temporal Causality Reward ($\mathcal{R}_{\text{temp}}$). The temporal causality reward ($\mathcal{R}_{\text{temp}}$) assesses the physical and logical coherence of the generated video’s dynamics. A video that successfully achieves the goal but does so through impossible or nonsensical motion is penalized. This 2.0-point metric, $\mathcal{R}_{\text{time}} = \mathcal{R}_{\text{phys}} + \mathcal{R}_{\text{logic}}$, evaluates the plausibility of the how. The Physics Plausibility score ($\mathcal{R}_{\text{phys}}$) scrutinizes the sequence for adherence to real-world physical principles, such as momentum, gravity, and object permanence, penalizing unrealistic motion or object interactions. Complementarily, the Causal Logic score ($\mathcal{R}_{\text{logic}}$) ensures that all state changes (effects) are preceded by logical and visible interactions (causes), such as an agent’s hand grasping an object before it moves, thereby preventing spurious correlations or "action-at-a-distance" phenomena.

Perceptual Fidelity Reward (\mathcal{R}_{per}). This score is computed as the sum of three clipped and normalized components, $\mathcal{R}_{\text{PSNR}}$, \mathcal{R}_{FVD} , and $\mathcal{R}_{\text{LPIPS}}$, each contributing a maximum of $\frac{2}{3}$ points. PSNR measures low-level, pixel-based reconstruction fidelity, LPIPS assesses perceptual similarity by comparing deep features in a manner aligned with human judgment, and FVD is a distributional metric that evaluates the overall realism of both visual appearance and temporal motion against a set of real videos.

C. X-Ego Details

We introduce X-Ego, the first large-scale dataset and benchmark designed to evaluate the capability of egocentric world models to synthesize complex, goal-directed scenes from sparse static context. X-Ego is constructed from the Nymeria [45] and Ego-Exo4D [22] datasets. We segment the videos based on the action annotations provided with these two datasets, resulting in clips that are uniformly 10 seconds long. We then instruct an expert temporal-action summarizer to generate concise descriptions of stationary atomic actions lasting 10 seconds. The summarizer is specifically constrained to select hand-on-object manipulations while strictly avoiding non-stationary actions, locomotion, speech, and idle states, relying primarily on the provided filtered annotations to ensure the selected action dominates the segment. This setup guarantees that the synthesized descriptions focus exclusively on fine-grained in-place manipulation tasks.

To gain a deeper understanding of human-environment interaction, we enrich this benchmark with dense annotations that detail fine-grained hand-object dynamics, object state changes, and step-level semantics. Instead of simple textual expansion, we instruct a multimodal language model to refine the concise atomic action description by grounding it in the actual video content, ensuring that the generated caption strictly adheres to the visual evidence. The output follows a structured four-sentence format, sequentially detailing the initial visual setup, the micro-dynamics of the motion, the physical reaction of the object, and the final outcome. The full dataset comprises 15,000 training samples, from which we sample 100 videos to serve as a standardized test set for evaluation. The test set contains carefully selected samples that span the benchmark’s interaction taxonomy, balancing broad coverage with the cost of evaluating long-horizon,

high-fidelity video generation under multiple complementary metrics.

D. Video Generation Evaluation

As introduced in §4.1, we employ a comprehensive suite of metrics to evaluate the performance of EgoForge on the X-Ego benchmark, and here we provide further detail on how each metric is computed. For semantic and perceptual alignment, we compute the **DINO-Score** to evaluate frame-level semantic similarity, which is calculated as the average cosine similarity between the DINOv2 ViT-g embeddings of the predicted video frames and the ground-truth video frames. We also compute the **CLIP-Score** to measure text-video alignment. This is calculated as the cosine similarity between the CLIP embedding of the generated video frames and the embedding of the corresponding textual guidance. Additionally, **LPIPS** (Learned Perceptual Image Patch Similarity) assesses perceptual distance by computing the L_2 distance between deep features extracted from a pretrained network (e.g., VGG), aligning more closely with human judgments of visual similarity than pixel-based metrics. For low-level visual fidelity, **PSNR (Peak Signal-to-Noise Ratio)** measures pixel-level reconstruction quality by comparing the maximum possible pixel value to the Mean Squared Error (MSE) between the generated and ground-truth frames, where a higher PSNR indicates lower pixel-wise error. **SSIM (Structural Similarity Index)** assesses visual fidelity by comparing three components: luminance, contrast, and structural information between the generated and ground-truth frames. Finally, for distributional and temporal fidelity, **FVD (Fréchet Video Distance)** assesses distributional realism by measuring the Fréchet Inception Distance between distributions of real and generated videos. Features are extracted from a pretrained video classification model, and the distance between the two multivariate Gaussian distributions (one for real videos, one for generated) is computed. **Flow MSE** measures temporal and motion fidelity. We first compute the optical flow fields for both the generated and ground-truth video sequences, and the metric is then the Mean Squared Error (MSE) calculated between these two sets of flow fields, penalizing discrepancies in predicted motion.

E. Visualization Results

We provide extensive visualization examples in Figure 7 to further demonstrate the generative capabilities of EgoForge. Across diverse tasks, including tabletop manipulation, deformable-object interaction, navigation on a climbing wall, ball throwing, and close-range assembly, the generated rollouts maintain a coherent first-person viewpoint, preserve scene layout over extended horizons, and exhibit plausible task-directed motion. Across examples, EgoForge maintains a stable first-person viewpoint and preserves the underlying scene structure while the action unfolds over time. In manipulation-heavy tasks such as cracking an egg, tearing adhesive tape, chopping onions, or installing a drawer handle, the generated frames show sustained hand-object interaction within a consistent workspace, with objects and surfaces remaining spatially coherent throughout the sequence. For deformable or large objects, such as folding a blanket, the model preserves the object’s presence and interaction region over extended horizons. In more dynamic scenarios like rock climbing or shooting a basketball, the rollouts exhibit clear temporal progression toward visually identifiable goals while maintaining consistent environment geometry, including climbing holds and the basketball hoop. These examples highlight the ability of EgoForge to generate temporally coherent, goal-directed egocentric sequences that sustain interaction dynamics and scene consistency over long durations.

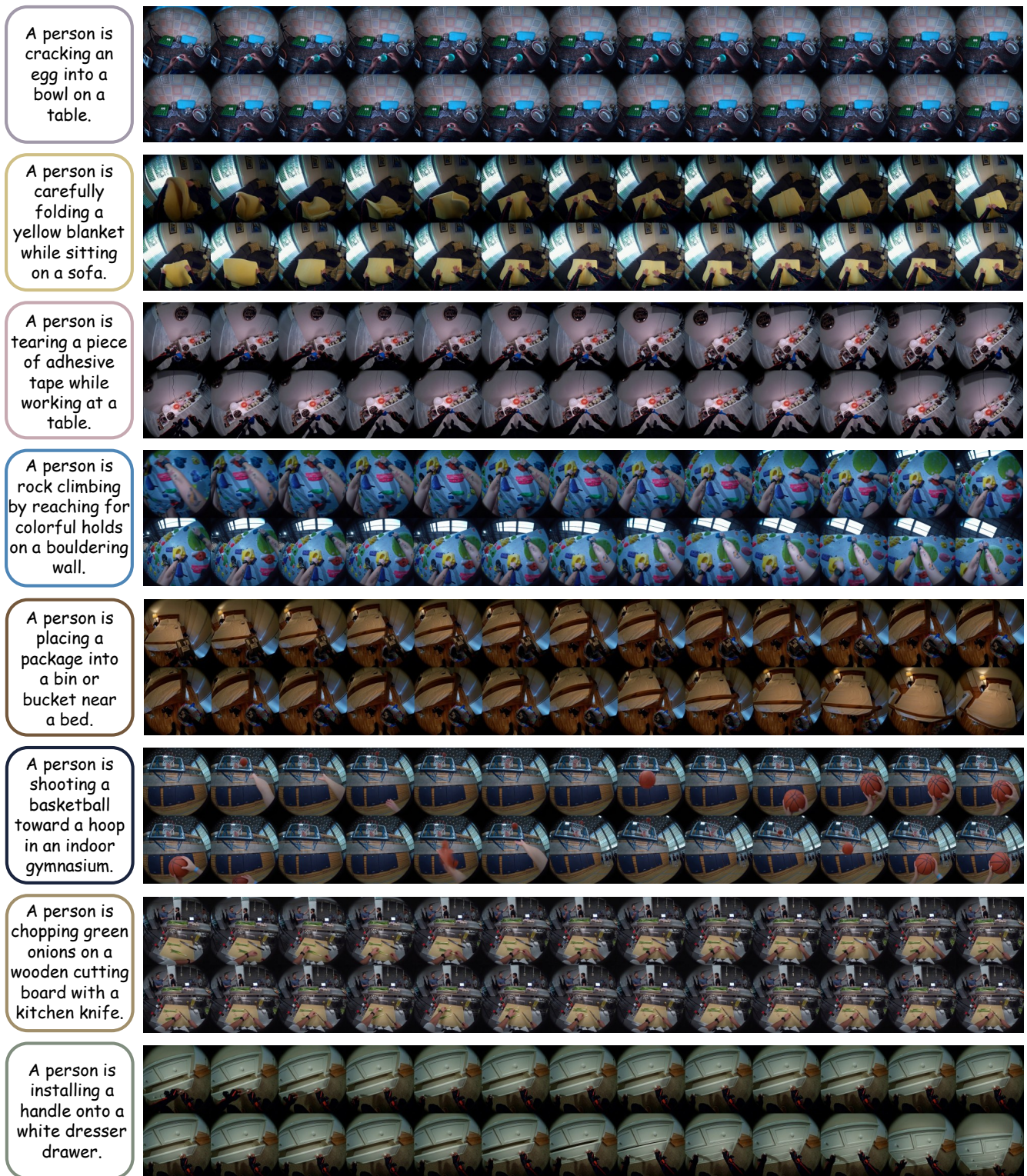


Figure 7: Dense visualization of a long-duration sequence. We present 26 frames from each video generated by EgoForge to highlight the seamless transitions and stable dynamics in complex ego-centric tasks.



Figure 8: DigiLens ARGO Smart glasses

F. Device for Real World Experiments

For our real-world experiments, we utilized the DigiLens ARGO smartglasses, as shown in Figure 8, to capture egocentric video data in real-world settings. The ARGO smartglasses employ Augmented Reality (AR) technology, which creates a visual overlay on the real world seen through the transparent display. This device is an enterprise-grade standalone system leveraging DigiLens’ core waveguide technology and is designed for industrial and enterprise use cases. The ARGO provides several key technical advantages for high-quality data capture, including a 48MP camera with autofocus, optical image stabilization (OIS), and electronic image stabilization (EIS), supporting 4×4 pixel binning and enhanced low-light performance. It also features a sophisticated five-microphone beamforming array designed to pick up the wearer’s voice in noisy environments and provides integrated stereo spatial audio recordings. The device runs on the Qualcomm Snapdragon XR2 Platform, providing standalone full mobile compute power. The use of the ARGO smartglasses is critical to our paper because it allows EgoForge to be tested for robust performance in real-world, out-of-domain (OOD) settings, addressing a limitation of previous egocentric world models. The high-fidelity data captured by the ARGO’s advanced sensor suite provides the essential grounding needed for EgoForge to reliably transfer visual cues and follow high-level semantic intent, producing coherent and controllable rollouts despite significant real-world variability.

Prompt for VideoDiffusionNFT Reward

You are an expert evaluator assessing goal achievement in egocentric video generation. Your task is to evaluate whether a generated first-person video successfully accomplishes a specified manipulation task by analyzing three dimensions: Goal Alignment, Environment Preservation, and Temporal Causality. You will evaluate a process video alongside its initial state image, target state image, and task description, providing quantitative scores for each dimension based on the criteria specified below.

The first task: Goal Alignment Scoring (Total 0–2.0 points)

Assess goal achievement through task completion analysis and semantic alignment between the video final state and the target state:

- **Task Completion Score:** Assign scores from 0.0 to 1.0 based on state transition analysis from initial to final frames, where 0.7~1.0 indicates all or most required state changes achieved, 0.4~0.6 indicates partial achievement with some changes incomplete, and 0.0~0.3 indicates minimal or no required changes with task not accomplished.
- **Visual Alignment Score:** Assign scores from 0.0 to 1.0 based on semantic correspondence between video final state and target image (accounting for first-person vs third-person viewpoint difference), where 0.7~1.0 indicates all or most target elements and spatial relationships present, 0.4~0.6 indicates some elements present with others missing, and 0.0~0.3 indicates minimal or no target elements present.

Provide a detailed breakdown for task completion and visual alignment.

You need to give the score with the following format:

```
{"score": [task completion score, visual alignment score]}
```

The second task: Environment Preservation Scoring (Total 0–2.0 points)

Assess environment consistency with initial state and resistance to target image contamination:

- **Consistency Score:** Assign scores from 0.0 to 1.0 based on environment consistency between initial and video states (ignoring target image environment which may differ), where 0.7~1.0 indicates all or most environmental features unchanged, 0.4~0.6 indicates some features consistent with moderate drift, and 0.0~0.3 indicates most features changed with major inconsistencies.
- **Contamination Score:** Assign scores from 0.0 to 1.0 based on freedom from target image environmental contamination, where 0.7~1.0 indicates no or minimal contamination with video maintaining original environment, 0.4~0.6 indicates moderate contamination with some target features leaked, and 0.0~0.3 indicates heavy contamination with video heavily influenced by target's different environment.

Provide a detailed breakdown for environmental consistency assessment.

You need to give the score with the following format:

```
{"score": [consistency score, contamination score]}
```

The third task: Temporal Causality Scoring (Total 0–2.0 points)

Assess whether the video demonstrates physically plausible and causally coherent progression from initial to final state:

- **Physics Plausibility Score:** Assign scores from 0.0 to 1.0 based on adherence to real-world physics, where 0.7~1.0 indicates all or most actions are physically realistic with proper gravity and motion, 0.4~0.6 indicates some actions are realistic with several implausibilities, and 0.0~0.3 indicates most actions violate physics with impossible movements.
- **Causal Logic Score:** Assign scores from 0.0 to 1.0 based on clarity of cause-effect relationships, where 0.7~1.0 indicates all or most actions have clear visible causes with logical sequences, 0.4~0.6 indicates some actions have visible causes with a partial causal chain, and 0.0~0.3 indicates most actions lack visible causes with broken logic.

Provide a detailed breakdown for each dimension.

You need to give the score with the following format:

```
{"score": [physics plausibility score, causal logic score]}
```

Caption Refinement Prompt for XEgo Dataset. The model takes both the original coarse caption and the video frames as input to generate a visually grounded fine-grained description.

You are an expert visual data annotator for ego-centric video datasets. Your task is to rewrite and refine a video text annotation by synthesizing the provided **Original Caption** with the actual **Video Content**.

Your Output Goal: A vivid, photorealistic description (3–4 sentences) that strictly aligns with the visual evidence in the video while maintaining the semantics of the original caption.

Instructions:

1. **Visual Grounding:** Analyze the Video Input first. Correct the Original Caption if it contradicts the visual evidence (e.g., wrong object color, wrong hand usage).
2. **Structure:**
 - **Sentence 1 (Setup):** Describe the visible appearance of the hands and objects (e.g., material, texture) based on the video start frame.
 - **Sentence 2 (Action):** Describe the fine-grained motion trajectory observed in the video clips.
 - **Sentence 3 (Reaction):** Describe the object’s physical response (deformation, displacement) shown in the video.
 - **Sentence 4 (Outcome):** Conclude with the final state visible in the end frame.
3. **Constraints:** Do not hallucinate details not present in the video.

Example Input:

- **Original Caption:** “The person pours water.”
- **Video Input:** [Sequence of frames showing a hand tilting a blue cup]

Example Output: “The person’s hand, gripping a ribbed blue plastic cup, tilts it sharply over a white bowl. A clear liquid cascades from the cup... [omitted for brevity] ...leaving droplets on the rim.”

Input Data:

Original Caption: {input_caption}

Video Input: <video_frames>

Video Segmentation Prompt for action localization

You are an expert temporal-action summarizer. You are given non-overlapping 10-second segments derived from a long video. Each segment includes:

- start and end: segment time in seconds (absolute timestamps from the video).
- raw: concatenated human annotations overlapping that 10-second window.
- filtered: the same annotations with any sentences containing disallowed categories removed, to highlight stationary/hand-object actions.

Your task:

1. Select 3 to 4 distinct stationary atomic actions across the timeline.
2. “Stationary” means the action is performed in place (hand/object manipulations are preferred).
3. The set of allowed stationary actions is NOT fixed. Infer candidate actions from the provided text (e.g., *shuffle, deal, draw, put, take, hold, open, close, align, sort, count, stack, fan, flip/turn over, organize, adjust, press, push, pull, slide, rotate an object, etc.*).
4. The following categories are strictly disallowed for selection as the main action: {disallowed_list}.
5. Avoid describing locomotion (walking/moving/stepping/running), speech (talking/speaking/chatting), or waiting/idle states.
6. Prefer segments where a single hand-on-object action clearly dominates the 10-second window. Use the “filtered” field primarily to judge this. If “filtered” is empty for a segment, skip it.
7. Each chosen output must represent a different action type (no duplicates). If the same action appears in multiple segments, choose only one representative segment.
8. For each selected segment, write exactly one concise English sentence that describes only the atomic action (single main verb phrase). Do not include walking, talking, or waiting. Avoid chaining multiple verbs. Keep it specific and objective (no speculation).
9. IMPORTANT: Use “the person” as the subject in all descriptions. Do NOT use “she”, “he”, “C”, or any other pronouns or names.

Formatting requirements:

- Output ONLY a JSON array (no other text).
- Each array element MUST be an object with keys: "start", "end", "text".
- "start" and "end" MUST copy the segment’s start and end values (integer timestamps in seconds).
- "text" MUST be a single English sentence describing only the stationary atomic action.
- Return exactly 5 to 8 objects. If fewer than 5 valid stationary actions exist, return as many as valid (possibly an empty array).

Segments JSON: {segments_json}